

# Fast Lithium Ion Diffusion in Brownmillerite $\text{Li}_x\text{Sr}_2\text{Co}_2\text{O}_5$

Xin Chen,<sup>1</sup> Xixiang Zhang,<sup>2</sup> Jie-Xiang Yu,<sup>1,3,\*</sup> and Jiadong Zang<sup>3,†</sup>

<sup>1</sup>*School of Physical Science and Technology, Soochow University, Suzhou 215006, China*

<sup>2</sup>*Physical Science and Engineering Division, King Abdullah University of*

*Science and Technology (KAUST), Thuwal 23955-6900, Kingdom of Saudi Arabia*

<sup>3</sup>*Department of Physics and Astronomy, University of New Hampshire, Durham, New Hampshire 03824, USA*

Transition metal oxides not only exhibits novel magnetic properties, but also provides outstanding ionic transports. Ionic conductors have great potential for interesting tunable physical properties via ionic liquid gating and novel energy storage applications such as all-solid-state lithium batteries. In particular, low migration barriers and high hopping attempt frequency are the keys to achieve fast ion diffusion in solids. Taking advantage of the oxygen-vacancy channel in  $\text{Li}_x\text{Sr}_2\text{Co}_2\text{O}_5$ , we show that migration barriers of lithium ion are as small as 0.28 ~ 0.17 eV depending on the lithium concentration rates. Our first-principles calculation also investigated hopping attempt frequency and concluded the room temperature ionic diffusivity and ion conductivity is high as  $10^{-7} \sim 10^{-6} \text{ cm}^2 \text{ s}^{-1}$  and  $10^{-3} \sim 10^{-2} \text{ S} \cdot \text{cm}^{-1}$  respectively, which outperform most of perovskite-type, garnet-type and sulfide Li-ion solid-state electrolytes. This work proves  $\text{Li}_x\text{Sr}_2\text{Co}_2\text{O}_5$  as a promising super-ionic conductor.

## I. INTRODUCTION

Ionic diffusion in solids has played a key role in not only manipulating many interesting physical properties in ion-electron-lattice-coupled systems via ionic liquid gating (ILG)[1–3], but also great potential applications in energy storage such as all-solid-state lithium batteries in which solid electrolytes with both high Li-ion conductivity and low electron conductivity[4–6]. To achieve highly efficient ionic diffusion, high ion conductivity or high ionic diffusivity is required. According to Nernst-Einstein equation[5, 7–9], the relationship between ionic diffusivity  $D$  and ion conductivity  $\sigma_i$  in solids can be given by

$$\sigma_i = q^2 n D \beta \quad (1)$$

where  $q$  is the electric charge of conducting ion,  $n$  is the ionic carrier concentration and  $\beta = (k_B T)^{-1}$  is the Boltzmann factor, the inverse of the product of Boltzmann constant and temperature. Meanwhile, under kinetically ideal conditions, the diffusivity can also be described by ion hopping through a pathway with a hopping frequency derived by Vineyard in the classical limit[5, 9, 10]:

$$D = a^2 \nu^* \exp(-E_a \beta) \quad (2)$$

where  $a$  is the hopping distance between two neighbor stable sites,  $\nu^*$  is the hopping attempt frequency and  $E_a$  is the activation energy of ions or the migration barriers during the diffusion. To this end, the high hopping attempt frequency and the low migration barriers is crucial for fast ionic diffusion.

Perovskite-type oxide systems are promising candidates for all-solid-state lithium batteries due to their well ordered diffusion channels and the high Young's modulus[11]. Furthermore, the desirable combination of the complex electron-lattice-spin coupling, the strongly correlated  $d$ -electrons and

the multivalent transition metal ions in transition metal oxides brings about novel electronic and magnetic properties[12–14]. Similar to the perovskite-type oxides, the recent study on brownmillerite  $\text{Sr}_2\text{Co}_2\text{O}_5$  demonstrated that ILG could induce tri-state phase transformation from  $\text{Sr}_2\text{Co}_2\text{O}_5$  to perovskite  $\text{SrCoO}_3$  and  $\text{H}_2\text{Sr}_2\text{Co}_2\text{O}_5$  by the insertion of oxygen anions and hydrogen cations respectively[2]. Han *et al.*[15] also reported that the direction of the oxygen-vacancy channels can be well controlled. The well-ordered[16, 17] and controllable oxygen-vacancy channels in brownmillerite  $\text{Sr}_2\text{Co}_2\text{O}_5$  provide favorable conditions for fast ionic diffusion and storage of ions, bringing about applications in fuel cells and rechargeable batteries.

In this paper, we systemically studied the diffusion of  $\text{Li}^+$  ion in brownmillerite  $\text{Sr}_2\text{Co}_2\text{O}_5$  based on first-principles calculations. The injected  $\text{Li}^+$  cations can be stabilized inside the oxygen-vacancy channels to form  $\text{Li}_x\text{Sr}_2\text{Co}_2\text{O}_5$  ( $x = 0.0 \sim 1.0$ ). After confirming the chemical stability, we obtained the migration barrier of  $\text{Li}^+$  cations along the oxygen-vacancy channels as 0.28 ~ 0.17 eV  $\text{Li}^+$  depending on  $\text{Li}^+$  concentration rates. The low migration barrier is caused by the multi-bonding property of Li-O bonds, and is lower than most of the Perovskite-type Li-ion solid electrolytes. The corresponding diffusivity and conductivity at room temperature are obtained as  $10^{-7} \sim 10^{-6} \text{ cm}^2 \text{ s}^{-1}$  and  $10^{-3} \sim 10^{-2} \text{ S} \cdot \text{cm}^{-1}$  respectively. Such high ionic diffusivity and ion conductivity can be considered as a super-ionic conductor[18].

## II. METHODOLOGY

We performed density-functional theory (DFT) based calculations with projector augmented wave (PAW) pseudopotentials[19, 20] implemented in the Vienna ab initio simulation (VASP) package[21, 22]. The generalized gradient approximation in Perdew, Burke, and Ernzerhof formation[23] was used as the exchange-correlation energy. The PAW pseudopotential set one 2s electron on each Li atom, eight 3d and one 4s electrons on each Co atom, two 4s,

\* jxyu@suda.edu.cn

† jiadong.zang@unh.edu

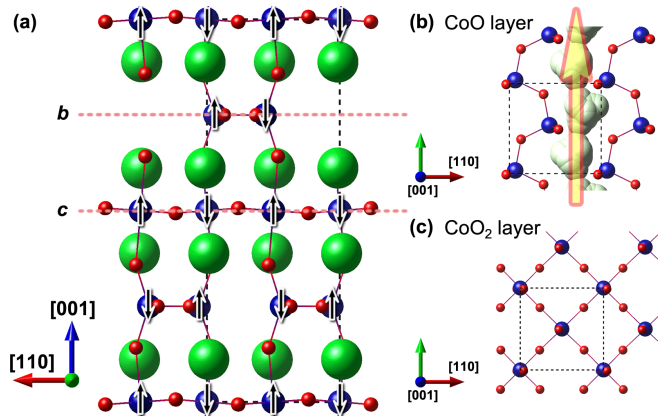


Figure 1. Crystal structure of  $\text{Sr}_2\text{Co}_2\text{O}_5$  in one unit cell. (a) The side view along  $[\bar{1}10]$  direction. Blue, red and green balls represent Co, O and Sr atoms respectively. The top view of the CoO layer and the CoO<sub>2</sub> layer in  $b$  and  $c$  are shown in (b) and (c) respectively. Black arrows in (a) shows the G-AFM spin-ordering. In (b) the connected region composed of light green spheres represents the area where a ball with a radius of a  $\text{Li}^+$  ion can be placed, so that the corresponding yellow arrow indicates the vacancy channel along the  $[\bar{1}10]$  direction in the CoO layer.

six  $4p$  and two  $5s$  electrons on each Sr atom, and two  $2s$  and four  $2p$  electrons on each O atom as the valence electrons. We employed the Hubbard  $U$  method in the Liechtenstein implementation[24] of  $U = 5.0$  eV,  $J = 0.9$  eV on Co( $3d$ ) orbitals to include the on-site strong-correlation effects of the localized  $3d$  electrons, by consulting the theoretical studies on the hydrogen-intercalated  $\text{Sr}_2\text{Co}_2\text{O}_5$ [2, 25]. An energy cutoff of 600 eV was used for the plane-wave expansion throughout the calculations. The  $k$ -points were sampled on a  $10 \times 10 \times 4$  Monkhorst-Pack mesh in the Brillouin zone of the unit cell of  $\text{Sr}_2\text{Co}_2\text{O}_5$  containing eight Co, eight Sr and twenty O atoms. All calculation results are converged when the total energy change and the band-structure-energy change between two self-consistent field steps are both less than  $10^{-8}$  eV. For structural relaxations we relaxed the atoms until the Hellmann-Feynman forces were less than  $1$  meV/Å.

In order to find the diffusion path and the corresponding migration barriers for Li diffusion in  $\text{Li}_x\text{Sr}_2\text{Co}_2\text{O}_5$ , we performed climbing image nudged elastic band (cl-NEB) calculations[26, 27] to find the saddle point and the minimum energy path between two stable local minimum. Eight images were employed and the force convergence is down to  $0.02$  eV/Å. Phonon modes of the diffused  $\text{Li}^+$  ions were obtained by using the finite displacement method[28] implemented in the Phonopy package[29].

### III. REVISIT STRUCTURAL, ELECTRONIC AND MAGNETIC PROPERTIES OF $\text{Sr}_2\text{Co}_2\text{O}_5$

*Structure* – The atomic structure of  $\text{Sr}_2\text{Co}_2\text{O}_5$  is shown in Fig.1. It has orthorhombic symmetry with space group  $Pma2$  (28). Compared to a  $\sqrt{2} \times \sqrt{2} \times 4$  perovskite supercell of

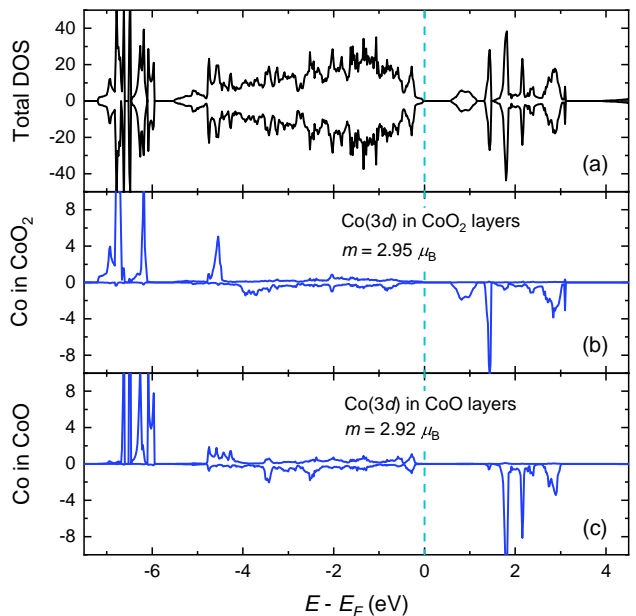


Figure 2. In the unit cell of  $(\text{Sr}_2\text{Co}_2\text{O}_5)_4$  under G-AF ordering, (a) the total density-of-state (DOS) and the projected DOS (PDOS) of Co( $3d$ ) in (b) CoO<sub>2</sub> layers and in (c) CoO layers. Positive and negative values represent the spin-majority (spin-up) and spin-minority (spin-down) channels respectively. The Fermi level is set to zero. The local spin magnetic moment on Co is also listed.

$\text{SrCoO}_3$ , the unit cell of  $\text{Sr}_2\text{Co}_2\text{O}_5$  containing eight Sr atoms, eight Co atoms and twenty O atoms loses four O atoms with two CoO layers ( $b$  in Fig. 1(a)) appearing. CoO layers shown in Fig. 1(b) have more spacing than CoO<sub>2</sub> layers Fig. 1(c). Once placing a ball with a radius of  $0.76$  Å, the ionic radius of  $\text{Li}^+$ , into the bulk, we then obtained a connected region composed of light green spheres, which is shown in Fig. 1(b). Periodic oxygen-vacancy channel structures are formed along the  $[\bar{1}10]$  direction so that they can provide two well-ordered diffusion channels per unit cell marked in Fig. 1(b). The calculated lattice constant for the orthorhombic unit cell with eight cobalt atoms, namely  $(\text{Sr}_2\text{Co}_2\text{O}_5)_4$  is  $a = 5.57$  Å,  $b = 5.46$  Å, and  $c = 16.00$  Å.

*Electronic and magnetic properties* – The total energy results show that  $\text{Sr}_2\text{Co}_2\text{O}_5$  has the ground state with G-type antiferromagnetic (G-AF) or rocksalt-type antiferromagnetism (AFM) spin ordering, consistent with previous studies[16]. G-AF is 68 meV per Co lower in energy than C-type AFM (C-AF) or column-type AFM, 101 meV lower than A-type AFM (A-AF) or layered-type AFM and 142 meV lower than ferromagnetic (FM) ordering. Therefore, the electronic structure of  $\text{Sr}_2\text{Co}_2\text{O}_5$  with G-AF ordering is investigated. According to the density-of-state (DOS) result shown in Fig. 2, a band gap about  $0.6$  eV indicates its insulating properties. In  $\text{Sr}_2\text{Co}_2\text{O}_5$ , O anions and Sr cations have the stable valence state  $-2$  and  $+2$  respectively, so that Co cations have valence state  $+3$  with six  $d$  electrons ( $d^6$ ) in principle. Thus, the high-spin state of  $\text{Co}^{3+}$  is  $S = 2$  which should have  $4.0 \mu_B$  local magnetic mo-

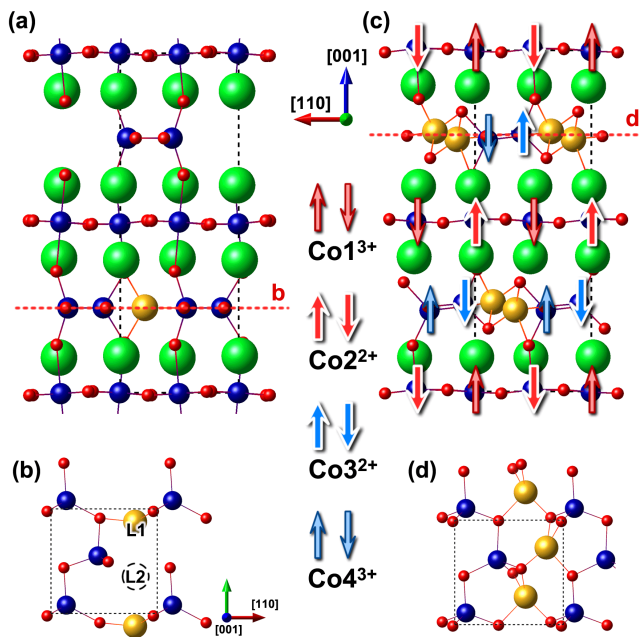


Figure 3. Crystal structures of  $\text{Li}_{0.25}\text{Sr}_2\text{Co}_2\text{O}_5$  with one Li atoms (yellow balls) per unit cell placed in (a) the side view and (b) the top view, and  $\text{LiSr}_2\text{Co}_2\text{O}_5$  with four Li atoms per unit cell placed in (c) the side view and (d) the top view. The dashed lines in side views are the CoO layers for top views. In (b), two stable sites L1 and L2 are listed. In (c) the G-AF spin ordering with four non-equivalent cobalt atoms is displayed. Co1 and Co4 are in the +3 valence state and Co2 and Co3 are in the +2 valence state.

ment with five spin-majority and one spin-minority  $d$  electrons. According to PDOS result in Fig. 2(b)(c), The featured  $\text{Co}(3d)$  in both  $\text{CoO}_2$  and  $\text{CoO}$  layers are all below the Fermi level in the spin-up channel, indicating Co's are indeed in the high-spin state. However, the local moment obtained by DFT is only  $2.95 \mu_B$ . According to the onsite density matrices and the corresponding occupancy of both two types of Co, six orbitals - five in spin-majority and one in spin-minority - are fully occupied with occupancy closed to 1, while other four orbitals have occupancy  $0.12 \sim 0.48$ , indicating unoccupied  $3d$  orbitals but hybridized with oxygen ligands under the ligand field. Such high Co-O hybridization leads to  $\text{Co}^{2+}\underline{L}$  state where the underline  $\underline{L}$  refers to a ligand hole[16, 30]. To this end,  $d^6$  configuration with  $S = 2$  high spin state on all  $\text{Co}^{3+}$  is still justified.

#### IV. LITHIUM-INJECTED $\text{Li}_x\text{Sr}_2\text{Co}_2\text{O}_5$

**Structures** – We now investigated the situations where Li atoms are injected into  $\text{Sr}_2\text{Co}_2\text{O}_5$ . With one Li placed in the unit cell, the most stable structure of  $\text{Li}_{0.25}\text{Sr}_2\text{Co}_2\text{O}_5$ , labeled as L1, is shown in Fig.3(a)(b). One Li atom is located in the spacing of a CoO layer, at a hollow site in the center of one oxygen-vacancy channel and have bonds with surrounding three O atoms. The Li-O bond-length is  $1.86 \text{ \AA}$ ,  $1.97 \text{ \AA}$  and  $1.99 \text{ \AA}$  respectively, close to the bond-length about

$2 \text{ \AA}$  in lithium oxides[31, 32]. It is distinct from the protonated  $\text{H}_x\text{Sr}_2\text{Co}_2\text{O}_5$  where each injected  $\text{H}^+$  cation is located next to an oxygen atom with a strong O – H bond so that  $\text{H}^+$  cations are not in the same plane with CoO layers[2, 25]. The other meta-stable structure, labeled as L2, where the Lithium ion is located in the middle of two neighboring most stable sites is also identified, shown in Fig.3(b). This meta-stable state is about  $0.16 \text{ eV}$  higher in energy than L1, the most stable one. Thus, it is obvious that each oxygen-vacancy channel in a  $(\text{Sr}_2\text{Co}_2\text{O}_5)_4$  unit cell can accommodate two Li atoms, so that at most four Li atoms can be placed to form  $\text{LiSr}_2\text{Co}_2\text{O}_5$ , shown in Fig.3(c)(d). With four Li atoms injected in the unit cell, the lattice constant for  $\text{LiSr}_2\text{Co}_2\text{O}_5$  are  $a = 5.72 \text{ \AA}$ ,  $b = 5.50 \text{ \AA}$  and  $c = 16.75 \text{ \AA}$ , only about 8.2% expansion in volume. This volume expansion is the result of the lattice, which has been internally compressed by the-injected lithium ions, releasing stress.

We have also investigated the lattice expansion of the structure under different fractional concentrations of lithium ions. With one Li atom in the unit cell, the volume of  $\text{Li}_{0.25}\text{Sr}_2\text{Co}_2\text{O}_5$  is expand about 2.4%. With three Li atoms intercalated, the volume expansion of  $\text{Li}_{0.75}\text{Sr}_2\text{Co}_2\text{O}_5$  is about 7.8%. For the case of inserting two lithium atoms, there are three non-equivalent configurations. The first one is where both lithium atoms are within the same oxygen-vacancy channel (labeled as L11). The second one involves two lithium atoms located in different oxygen-vacancy channels and arranged in a staggered pattern (labeled as L12a). The third configuration finds each lithium atom occupying a different oxygen-vacancy channel, positioned on the same side (labeled as L12b). The volume expansions are 5.0% for L11, 5.2% for L12a, 5.3% for L12b respectively. The detailed lattice parameters for each structure configurations are listed in Table IV. As expected, the volume expansion is essentially linearly related to the concentrations of lithium ions.

**Stability** – The chemical stability can be confirmed by the formation energy of  $\text{Li}_x\text{Sr}_2\text{Co}_2\text{O}_5$  from bulk  $\text{Sr}_2\text{Co}_2\text{O}_5$  and Lithium metal, which is defined by

$$E_f = E_{\text{Li}_n(\text{Sr}_2\text{Co}_2\text{O}_5)_4} - nE_{\text{Li}} - E_{(\text{Sr}_2\text{Co}_2\text{O}_5)_4} \quad (3)$$

where  $n = 4x$  is the number of Li placed in the  $(\text{Sr}_2\text{Co}_2\text{O}_5)_4$  unit cell and the total energy for face-centered cubic Li lattice is used for  $E_{\text{Li}}$ . The formation energy results for  $n = 1, 3, 4$  are

Table I. The calculated lattice constants for  $\text{Li}_x\text{Sr}_2\text{Co}_2\text{O}_5$  with the various concentration of Li ions ( $x = 0.25, 0.5, 0.75, 1.0$ ). For  $x = 0.5$ , there are three non-equivalent structures labeled L11, L12a and L12b respectively (see main text).

	$a$ ( $\text{\AA}$ )	$b$ ( $\text{\AA}$ )	$c$ ( $\text{\AA}$ )
$x = 0.25$	5.66	5.50	16.02
$x = 0.5$ (L11)	5.66	5.45	16.58
$x = 0.5$ (L12a)	5.67	5.45	16.56
$x = 0.5$ (L12b)	5.65	5.46	16.65
$x = 0.75$	5.69	5.51	16.73
$x = 1.0$	5.72	5.50	16.75

$-2.01$ ,  $-5.60$  and  $-7.98$  eV per unit cell respectively. Those for all three non-equivalent  $n = 2$  situations are  $-2.93$ ,  $-3.20$  and  $-3.74$  eV respectively. They are all negative, indicating the system reduce energy when  $\text{Li}_x\text{Sr}_2\text{Co}_2\text{O}_5$  formed with the injected Li atoms. The injected Li atoms can be stabilized in the oxygen-vacancy channels in all the cases of various concentration rates. Since the formation energy monotonically decreases with the increasing concentration of Li ions, one can deduce that once Li ions start to penetrate into  $\text{Sr}_2\text{Co}_2\text{O}_5$ , the ultimate quasi-static configuration should be full occupancy, which means the situation where four lithium ions per unit cell are present.

**Electronic and magnetic properties** – To investigate how lithium’s injection affect the electronic structure and magnetic ordering, we therefore focus on  $\text{LiSr}_2\text{Co}_2\text{O}_5$  with all four hollow sites in the unit cell occupied by Li atoms to maximum the effect. Since each  $\text{Li}^+$  cation has valence state +1, the average valence state of Co is +2.5. In that case, half of Co are +3 with  $d^6$  and half are +2 with  $d^7$ . The total energy results still show that the G-AF spin ordering with zero net magnetization still has the lowest total one. G-AF is 11 meV per Co lower in energy than C-AF, 12 meV lower than A-AF and 18 meV lower than the FM ordering. Therefore, in G-AF spin ordering, four Co ions in the unit cell has spin-up local spin magnetic moment and other four are spin-down. The corresponding DOS and PDOS on four spin-up Co ions labeled Co1, Co2, Co3 and Co4 are shown in Fig.4. The total DOS gives a band gap about 0.8 eV indicating the insulating properties. The local spin magnetic moments, Co1 and Co2 in  $\text{CoO}_2$  layers are  $1.83 \mu_B$  and  $2.73 \mu_B$  respectively, and those on Co3 and Co4 in CoO layers are  $2.62 \mu_B$  and  $2.97 \mu_B$  respectively. According to PDOS results of Co, Co1(3d) in  $\text{CoO}_2$  layers (Fig. 4(b)) has unoccupied states above the Fermi level in the spin-up channel, indicating that Co1 is not in the high spin state. On the other hand, a sharp peak appears around  $-4.5\text{eV}$  below the Fermi level in the spin-down channel, indicating that Co1 has more occupied state in the spin-down channel than  $\text{Co}^{3+}$  in  $\text{Sr}_2\text{Co}_2\text{O}_5$ . Co2(3d) in  $\text{CoO}_2$  layers (Fig.4(c)) and Co3(3d) in CoO layers (Fig.4(d)) has fully occupied state in the spin-up channel while in the spin-down channel, the unoccupied state is located around  $3.0 \sim 4.0\text{eV}$  above the Fermi level, 1.0 eV higher than the unoccupied state of  $\text{Co}^{3+}$  in  $\text{Sr}_2\text{Co}_2\text{O}_5$ . It indicates that  $d$  electrons on Co2 and Co3 in  $\text{LiSr}_2\text{Co}_2\text{O}_5$  meet stronger on-site Coulomb interaction with more  $d$  electrons than on  $\text{Co}^{3+}$  in  $\text{Sr}_2\text{Co}_2\text{O}_5$ . PDOS of Co4 in CoO layers (Fig.4(e)) are similar to that of Co in  $\text{Sr}_2\text{Co}_2\text{O}_5$ .

We also examined the onsite density matrices and the corresponding occupancies of all the four types of Co ions. For Co1 in  $\text{CoO}_2$  layers, four orbitals in spin-majority and two in spin-minority are occupied with occupancies close to 1, and others have occupancies  $0.12 \sim 0.48$ , indicating unoccupied 3d orbitals which only have hybridization bonding-states with the surrounding oxygen ligands. Therefore, Co1 has +3 valence state and  $d^6$  configuration with  $S = 1$  intermediate spin state. For Co2 in  $\text{CoO}_2$  layers and Co3 in CoO layers, five orbitals in spin-majority and two in spin-minority are occupied with occupancies close to 1, so that they are both in +2 valence state and  $d^7$  configuration with  $S = 3/2$  high spin

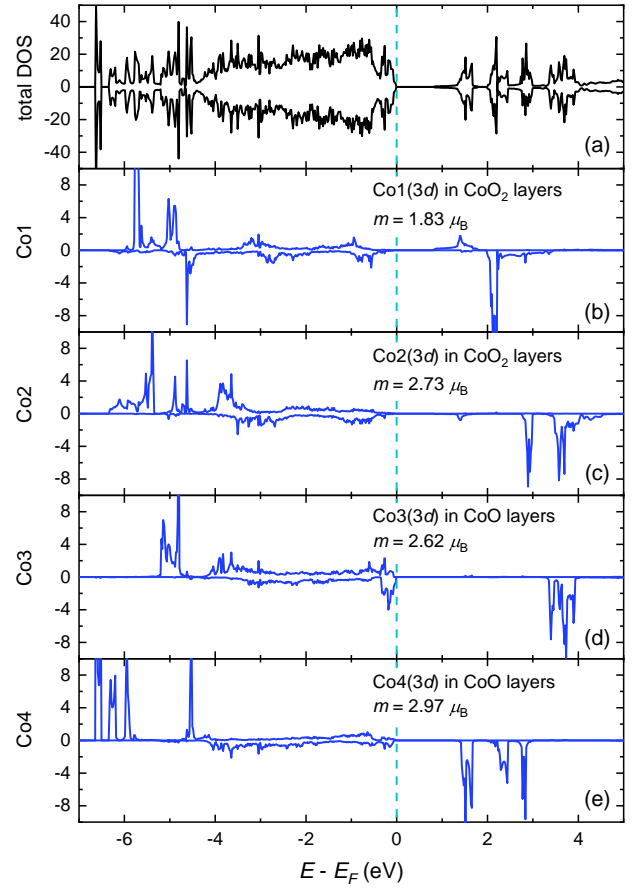


Figure 4. In the unit cell of  $(\text{LiSr}_2\text{Co}_2\text{O}_5)_4$  in G-AF ordering, (a) the total DOS and the PDOS of 3d orbitals of Co1, Co2, Co3 and Co4 which is the four Co atoms with positive local spin magnetic moments in the unit cell.

state. For Co4 in CoO layers, five orbitals in spin-majority and one in spin-minority are occupied with occupancies close to 1, so that Co4 are in +3 valence state and  $d^6$  configuration with  $S = 2$  high spin state. Such metal segregation is caused by the multivalent cobalt ions, and happens in other lithium-rich materials[33, 34] The spin texture of G-AF ordering is therefore displayed in Fig.3(c). The insulating properties and the G-AF spin ordering ground state are also confirmed in the electronic structures of  $\text{Li}_x\text{Sr}_2\text{Co}_2\text{O}_5$  with  $x = 0.25, 0.5$  and  $0.75$ . Due to the multivalent cobalt cations,  $\text{Li}^+$ -injection  $\text{Li}_x\text{Sr}_2\text{Co}_2\text{O}_5$  does not affect the insulating properties and the antiferromagnetic ordering.

## V. DIFFUSION PROPERTIES OF LI IN $\text{Li}_x\text{Sr}_2\text{Co}_2\text{O}_5$

**Migration barriers** – To investigate the diffusion of  $\text{Li}^+$  cations in  $\text{Li}_x\text{Sr}_2\text{Co}_2\text{O}_5$ , we first calculated the migration barriers of  $\text{Li}^+$  cations with various Li concentration  $x$  in  $\text{Li}_x\text{Sr}_2\text{Co}_2\text{O}_5$ . We considered two extreme cases. The first is  $\text{Li}_{0.25}\text{Sr}_2\text{Co}_2\text{O}_5$ , which mimics the situation when  $\text{Li}^+$  cations just begin to insert into  $\text{Sr}_2\text{Co}_2\text{O}_5$  so that very few  $\text{Li}^+$  cations

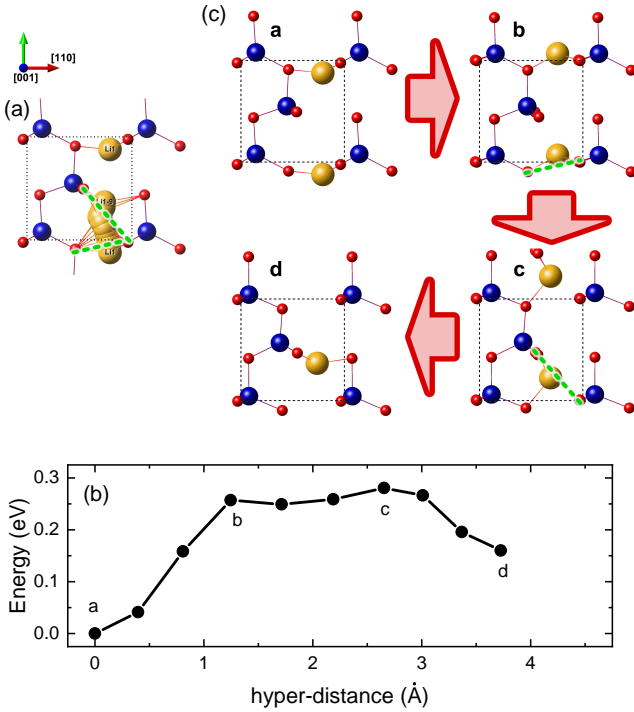


Figure 5. cl-NEB results of one Li diffusion in the unit cell of  $\text{Li}_{0.25}\text{Sr}_2\text{Co}_2\text{O}_5$ . (a) the top view of the migration path of the Li ion diffusing from site L1 to L2 (structure configuration a and d in (c) respectively). (b) The total energies of each state relative to the initial state as a function of hyper-distances between each intermediate image and the initial state. (c) the top view of the intermediate images labeled in (b). The dashed green lines in (a) and (c) show the two gates composed of two nearby oxygen atoms.

are injected in the  $\text{Sr}_2\text{Co}_2\text{O}_5$ . To this end, we employed the lattice constant of  $\text{Sr}_2\text{Co}_2\text{O}_5$  for this unit cell. Therefore, we set the two stable structural configurations L1 and L2 as the initial and ending states. The other scenario is the opposite, considering the condition of almost full occupancy of Li ions. According to the analysis in Section IV, this situation corresponds to the state with the lowest formation energy, which is the quasi-static one after Li ions insertion. To describe the ionic carriers, analogous to the "holes" in p-type electronic semiconductors, we employed  $\text{Li}_{0.75}\text{Sr}_2\text{Co}_2\text{O}_5$  with three Li atoms in the unit cell. For the lattice constant, we used the value of the full occupancy, that is, the  $\text{LiSr}_2\text{Co}_2\text{O}_5$  configuration, to calculate the migration barrier of the Li ion in the oxygen-vacancy channel which is not fully occupied. Two different hole positions provide the initial and ending states. Then, other eight intermediate images on the diffusion pathway are used to find the lowest migration barriers using cl-NEB calculations.

The migration results for  $\text{Li}_{0.25}\text{Sr}_2\text{Co}_2\text{O}_5$  are shown in Fig.5. The migration path is straightforward; the diffused Li ion starts from the initial state and follows an almost straight path along the oxygen-vacancy channel to reach the ending state. From Fig.5(a) and (c), it can be observed that the migration path passes through two gates composed of two oxygen

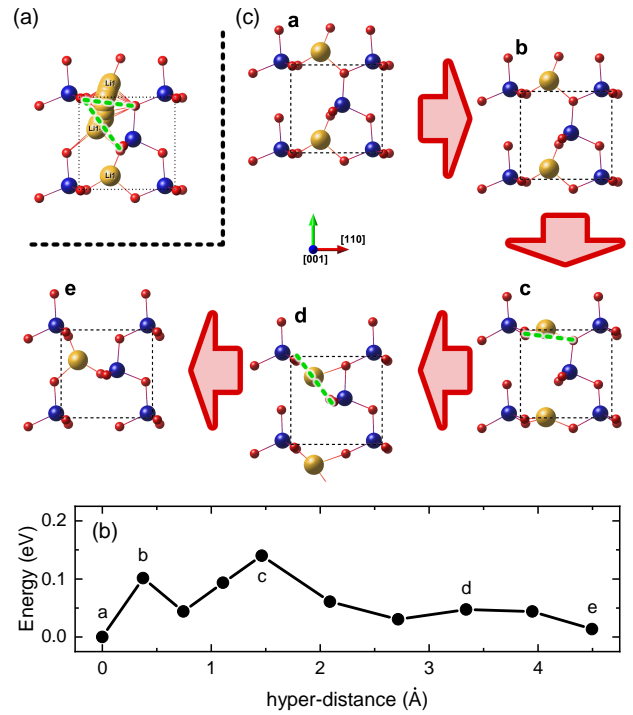


Figure 6. cl-NEB results of one Li diffusion in the unit cell of  $\text{Li}_{0.75}\text{Sr}_2\text{Co}_2\text{O}_5$ . (a) the top view of the migration path. (b) The total energies of each state relative to the initial state as a function of hyper-distances between each intermediate image and the initial state. (c) the top view of the intermediate images labeled in (b). The dashed green lines in (a) and (c) show the two gates composed of two nearby oxygen atoms.

atoms each, which are the main obstacles during ion migration. Consequently, in Fig.5(b), we see that the intermediate states b and c correspond to the states near the two gates, with their potential energy at local maximum. Among them, state c has the highest potential energy, which is where the migration barrier of the entire migration path is located, with a magnitude of 0.28 eV.

The results for  $\text{Li}_{0.75}\text{Sr}_2\text{Co}_2\text{O}_5$  are shown in Fig.6. Similar to the case of  $\text{Li}_{0.25}\text{Sr}_2\text{Co}_2\text{O}_5$ , the migration path here also essentially takes a straight-line form from the initial state to the ending state. Due to the presence of the two gates composed of oxygen atoms, intermediate states c and d in Fig6(b) are the two local maxima on the migration path. Interestingly, intermediate state b is also a local maximum, which will be analyzed later. Among them, the potential energy at the intermediate state c is the highest and is considered to be the migration barrier of 0.17 eV for the entire migration path. This magnitude of migration barrier is similar with or even lower than that of  $\text{H}^+$  diffusion in the protonated  $\text{H}_x\text{Sr}_2\text{Co}_2\text{O}_5$  ( $\sim 0.3$  eV)[25]. It is also significantly lower than most of the migration barriers of the perovskite-type Li-ion solid electrolytes (0.6  $\sim$  0.2 eV)[11].

To obtain the origin of the low migration barriers of  $\text{Li}_x\text{Sr}_2\text{Co}_2\text{O}_5$ , we investigated the bonding properties between Li and O during the diffusion. Fig.7 shows the charge differ-

ence between the initial state and intermediate/ending states. The change of the spatial charge distribution illustrates the change of the chemical bonds during the diffusion, so that the directions and sizes of isosurfaces can be used to estimate the directions and the strength of the interaction between the diffused ion and the neighboring atoms. In the case of  $\text{Li}_{0.25}\text{Sr}_2\text{Co}_2\text{O}_5$ , the diffused Li ion in the intermediate state b has a strong bond interaction, shown as a red arrow in Fig.7(a), though the Li-O distance is about  $2.70\text{\AA}$  which is much larger than the normal Li-O bonds. The situation for the intermediate state c is similar to that of intermediate state b, where the Li ion has already formed chemical bonds with the subsequent oxygen atoms upon diffusing to that position, yet the interaction with the preceding oxygen atom has not been severed, as indicated by the red arrow in Fig.7(a). The newly formed bonds compensate the energy cost of broken bonds, eventually reducing the migration barriers. In the case of  $\text{Li}_{0.75}\text{Sr}_2\text{Co}_2\text{O}_5$ , on the other hand, the intermediate state b exhibits the opposite effect. Due to the significant offset of the diffusing Li ion from the center of the oxygen-vacancy channel, the distance between this lithium ion and the oxygen atom on one side is relatively large, approximately  $2.83\text{\AA}$ , resulting in a noticeably weakened interaction, which can be considered as the breaking of the Li-O bond, as indicated by the green arrow in Fig.7(b). It can be inferred that the energy required for this broken Li-O bond is the main reason for the significant increase in the total energy of the intermediate state b. In all other respects, the situation is similar to  $\text{Li}_{0.25}\text{Sr}_2\text{Co}_2\text{O}_5$ , meaning that the additional Li-O bond can lower the energy of the intermediate state during the migration.

*Hopping attempt frequency, ionic diffusivity and ion conductivity* – The ionic diffusivity/conductivity in a solid depends not only on the migration barriers but also on the pre-exponential factor  $a^2\nu^*$  in Eq.2. According to Vineyard formula[10, 35], the hopping attempt frequency can be given by

$$\nu^* = \frac{\prod_{i=1}^N \nu_i^0}{\prod_{j=1}^{N-1} \nu_j^s} \quad (4)$$

where  $\nu_i^0$  and  $\nu_j^s$  are the normal frequencies at the  $\Gamma$  point of vibration modes of the initial and saddle point state respectively, and  $N$  is the total number of phonon modes for the initial state. Notice that the number of normal modes in the product of saddle point is one less than that in initial state. That is because of the presence of an imaginary frequencies mode at the saddle point state caused by the instability along the diffusion direction. This mode needs to be removed from the product. The phonon modes at the  $\Gamma$  point for the initial and the saddle point state of both  $\text{Li}_{0.25}\text{Sr}_2\text{Co}_2\text{O}_5$  and  $\text{Li}_{0.75}\text{Sr}_2\text{Co}_2\text{O}_5$  were therefore calculated. As a result, the hopping attempt frequencies for  $\text{Li}_{0.25}\text{Sr}_2\text{Co}_2\text{O}_5$  and  $\text{Li}_{0.75}\text{Sr}_2\text{Co}_2\text{O}_5$  are 6.87 THz and 0.95 THz, respectively. The lower migration barrier usually leads to a smoother potential energy surface for diffusion, causing the lower force constant and the corresponding vibration frequency. So that the hopping attempt frequency for  $\text{Li}_{0.75}\text{Sr}_2\text{Co}_2\text{O}_5$  is lower than that for  $\text{Li}_{0.25}\text{Sr}_2\text{Co}_2\text{O}_5$ . The hopping distance is regarded as the half of the lattice constant

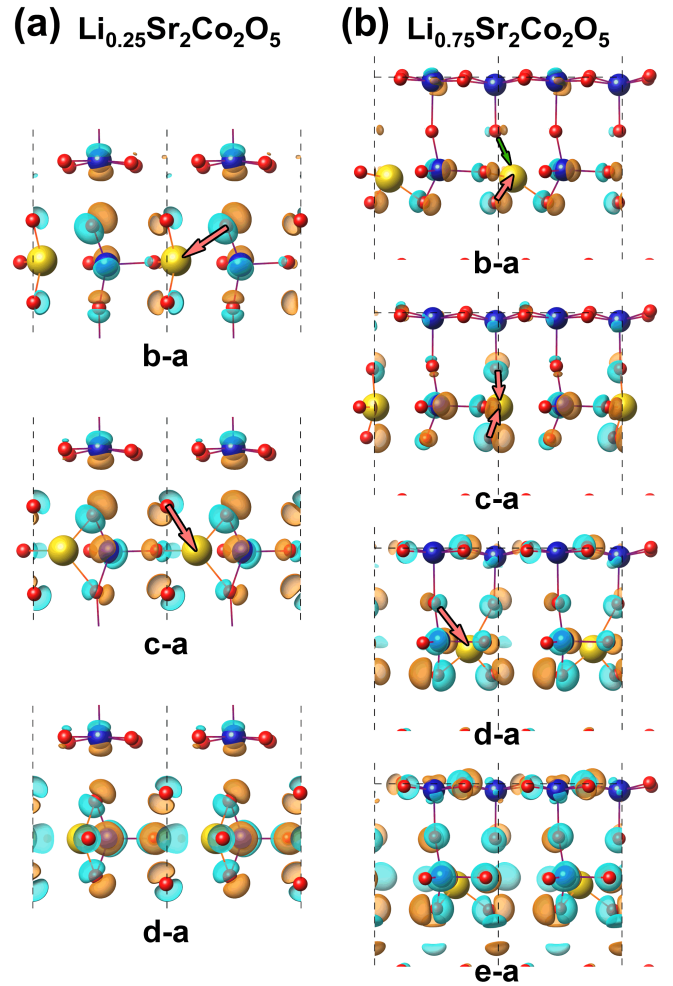


Figure 7. In the side views, the charge differences between the initial state (labeled a) and intermediate/ending states (labeled b-d for  $\text{Li}_{0.25}\text{Sr}_2\text{Co}_2\text{O}_5$  and b-e for  $\text{Li}_{0.75}\text{Sr}_2\text{Co}_2\text{O}_5$ ) for (a)  $\text{Li}_{0.25}\text{Sr}_2\text{Co}_2\text{O}_5$  and (b)  $\text{Li}_{0.75}\text{Sr}_2\text{Co}_2\text{O}_5$ . The labels corresponds to the label in Fig.5 and Fig.6. Orange and cyan isosurfaces correspond to positive and negative values respectively. The red and green arrows respectively represent the strong interactions that can lower the potential energies during the migration process and the weak interactions that cannot reduce the potential energies.

along  $[\bar{1}10]$  direction, which is  $2.75 \times 10^{-8}\text{cm}$  for both two phases. To this end, for  $\text{Li}_{0.25}\text{Sr}_2\text{Co}_2\text{O}_5$  and  $\text{Li}_{0.75}\text{Sr}_2\text{Co}_2\text{O}_5$ , we can estimate the pre-exponential factor of diffusivity  $a^2\nu^*$ , which is  $5.20 \times 10^{-3}\text{cm}^2\text{s}^{-1}$  and  $0.72 \times 10^{-3}\text{cm}^2\text{s}^{-1}$  respectively. The hopping attempt frequency can be regarded as the frequency that the diffused ions attempt to climb over the barrier, so that  $\nu^* \exp(-E_a/\beta)$  is nothing but the hopping frequency from one stable site to its neighbor site with a successful hopping. At room temperature with  $T = 300\text{K}$ ,  $\beta = k_B T = 38.7\text{eV}^{-1}$ , the ionic diffusivity  $D$  based on Vogel-Tammann-Fulcher model (Eq.2) is  $1.02 \times 10^{-7}\text{cm}^2\text{s}^{-1}$  and  $1.00 \times 10^{-6}\text{cm}^2\text{s}^{-1}$  respectively. If the ionic concentration  $n$  is regarded as one  $\text{Li}^+$  cation per unit cell, the corresponding ionic conductivity  $\sigma_i = q^2 n D \beta$  based on Eq.1 are therefore

$1.20 \times 10^{-3} \text{ S} \cdot \text{cm}^{-1}$  and  $1.17 \times 10^{-2} \text{ S} \cdot \text{cm}^{-1}$  respectively. The room temperature diffusivity and conductivity are both superior to most of the perovskite-type Li-ion solid electrolytes ( $10^{-4} \sim 10^{-3} \text{ S} \cdot \text{cm}^{-1}$  for bulk conductivity)[11], garnet-type solid-state electrolytes ( $10^{-4} \sim 10^{-3} \text{ S} \cdot \text{cm}^{-1}$ )[36], and sulfide solid electrolytes ( $10^{-7} \sim 10^{-3} \text{ S} \cdot \text{cm}^{-1}$ )[37, 38].

The above estimates of diffusivity and conductivity are based on an assumption that diffusion over each energy barrier is adiabatic, and the mechanical energy of the migrating lithium ion is conserved from the initial state to the final state. However, when there are several local maxima of the potential energy along the diffusion path, it is possible that after overcoming each local barrier, the lithium ion may reset its kinetic energy through scattering due to thermal fluctuations. Here, we consider a strong scattering limit where the lithium ion resets its kinetic energy after surmounting each local barrier. Thus, the diffusion path is divided into independent segments, with each segment's diffusivity calculated separately. For  $\text{Li}_{0.25}\text{Sr}_2\text{Co}_2\text{O}_5$ , the original diffusion path from point a to d in Fig.5(b) is split into two segments for overcoming the local barriers at b and c. The diffusion distances for these segments are  $1.95 \text{ \AA}$  and  $0.80 \text{ \AA}$ , respectively, and the corresponding relative barriers are  $0.26 \text{ eV}$  and  $0.03 \text{ eV}$ , respectively. Using the previously mentioned method, the hopping attempt frequencies are  $4.60 \text{ THz}$  and  $5.61 \text{ THz}$  respectively. Thus, the resulting diffusivity in the room temperature is  $0.75 \times 10^{-7} \text{ cm}^2 \text{ s}^{-1}$  and  $1.12 \times 10^{-4} \text{ cm}^2 \text{ s}^{-1}$ , respectively. Considering that the two segments are connected in series, with the second segment's diffusivity being much larger than the first, the overall conductivity is determined primarily by the first segment. Consequently, the resulting conductivity is calculated to be  $0.88 \times 10^{-3} \text{ S} \cdot \text{cm}^{-1}$ .

In the case of  $\text{Li}_{0.75}\text{Sr}_2\text{Co}_2\text{O}_5$ , the whole diffusion path can also be divided into three segments, corresponding to three local barriers at b, c and d in Fig.6. The relative barriers are  $0.10 \text{ eV}$ ,  $0.10 \text{ eV}$  and  $0.02 \text{ eV}$  respectively. The hopping attempt frequencies obtained are  $0.39 \text{ THz}$ ,  $0.95 \text{ THz}$  and  $7.09 \text{ THz}$  respectively. The corresponding diffusivity in the room temperature is  $1.65 \times 10^{-7} \text{ cm}^2 \text{ s}^{-1}$ ,  $3.51 \times 10^{-6} \text{ cm}^2 \text{ s}^{-1}$  and  $3.08 \times 10^{-4} \text{ cm}^2 \text{ s}^{-1}$  respectively. In the case of series connection, the overall conductivity is determined primarily only by the first and second segments, which is about  $1.85 \times 10^{-3} \text{ S} \cdot \text{cm}^{-1}$ .

Under the strong scattering limit, the calculated ionic conductivity for both cases has decreased, but it remains within the same order of magnitude. The actual situation would be between the cases of the adiabatic approximation and strong scattering. Considering that the diffusion length in a diffusion

period is only  $2.75 \text{ \AA}$ , the actual conductivity should be closer to the results of the adiabatic approximation.

## VI. CONCLUSIONS

In summary, We investigated the structural, electronic and magnetic properties of brownmillerite  $\text{Li}_x\text{Sr}_2\text{Co}_2\text{O}_5$  and confirmed the oxygen vacancy channels, the insulating property and the G-AF spin ordering ground state. At most four  $\text{Li}^+$  cations can be stabilized in the center of the oxygen vacancy channels of an orthorhombic  $(\text{Sr}_2\text{Co}_2\text{O}_5)_4$  unit cell to form  $\text{Li}_x\text{Sr}_2\text{Co}_2\text{O}_5$  ( $x = 0.0 \sim 1.0$ ). The G-AF spin ordering and insulating property is still remained with the lithium's injection. By employing cl-NEB calculations, we obtained the migration barriers of  $\text{Li}_x\text{Sr}_2\text{Co}_2\text{O}_5$  for  $x = 0.25$  and  $0.75$  as  $0.28 \text{ eV}$  and  $0.17 \text{ eV}$ , respectively. After obtaining the hopping attempt frequencies via Vineyard formula, we therefore obtained the corresponding diffusivity and conductivity at the room temperature as  $1.02 \times 10^{-7} \text{ cm}^2 \text{ s}^{-1}$  and  $1.20 \times 10^{-3} \text{ S} \cdot \text{cm}^{-1}$  for  $x = 0.25$  respectively, and  $1.00 \times 10^{-6} \text{ cm}^2 \text{ s}^{-1}$  and  $1.17 \times 10^{-2} \text{ S} \cdot \text{cm}^{-1}$  for  $x = 0.75$  respectively. The high ionic diffusivity and ion conductivity indicate brownmillerite  $\text{Sr}_2\text{Co}_2\text{O}_5$  as a promising super-ionic conductor. Because the structure of brownmillerite-type is very similar to that of the perovskite-type,  $\text{Li}_x\text{Sr}_2\text{Co}_2\text{O}_5$  inherits the advantages of the perovskite-type solid electrolyte, which include high Li-ion conductivity, low electron conductivity, and wide electrochemical window. In particular, due to the exclusive occupation of the oxygen vacancy channels by Li ions in  $\text{Li}_x\text{Sr}_2\text{Co}_2\text{O}_5$ , it can address the issue of poor stability against lithium metal faced by perovskite-type solid electrolytes[6, 11]. We expect that  $\text{Li}_x\text{Sr}_2\text{Co}_2\text{O}_5$  can be compatible with the application of perovskite-type solid electrolytes in all-solid-state lithium batteries.

## ACKNOWLEDGMENTS

We are grateful for fruitful discussions with Prof. Pu Yu. This work was financially supported by the National Natural Science Foundation of China (12274309). Analysis of magnetic states done at UNH was supported by the U.S. Department of Energy, Director, Office of Science, Office of Basic Energy Sciences, Division of Materials Sciences and Engineering under Contract No. DE-SC0020221. The cl-NEB calculations were performed at Shaheen II in King Abdullah University of Science and Technology (KAUST).

- 
- [1] A. J. Tan, M. Huang, C. O. Avci, F. Büttner, M. Mann, W. Hu, C. Mazzoli, S. Wilkins, H. L. Tuller, and G. S. D. Beach, *Nature Materials* **18**, 35 (2018).
- [2] N. Lu, P. Zhang, Q. Zhang, R. Qiao, Q. He, H.-B. Li, Y. Wang, J. Guo, D. Zhang, Z. Duan, Z. Li, M. Wang, S. Yang, M. Yan, E. Arenholz, S. Zhou, W. Yang, L. Gu, C.-W. Nan, J. Wu, Y. Tokura, and P. Yu, *Nature* **546**, 124 (2017).
- [3] Z. Li, S. Shen, Z. Tian, K. Hwangbo, M. Wang, Y. Wang, F. M. Bartram, L. He, Y. Lyu, Y. Dong, G. Wan, H. Li, N. Lu, J. Zang, H. Zhou, E. Arenholz, Q. He, L. Yang, W. Luo, and P. Yu, *Nature Communications* **11**, 184 (2020).
- [4] Y. Wang, B. Liu, Q. Li, S. Cartmell, S. Ferrara, Z. D. Deng, and J. Xiao, *Journal of Power Sources* **286**, 330 (2015).

- [5] D. Aksyonov, A. Boev, S. Fedotov, and A. Abakumov, *Solid State Ionics* **393**, 116170 (2023).
- [6] D. Wu, L. Chen, H. Li, and F. Wu, *Progress in Materials Science* **139**, 101182 (2023).
- [7] R. Kutner, *Physics Letters A* **81**, 239 (1981).
- [8] M. Park, X. Zhang, M. Chung, G. B. Less, and A. M. Sastry, *Journal of Power Sources* **195**, 7904 (2010).
- [9] M. Sotoudeh, S. Baumgart, M. Dillenz, J. Döhn, K. Forster-Tonigold, K. Helmbrecht, D. Stottmeister, and A. Groß, *Advanced Energy Materials* **14**, 2302550 (2023).
- [10] G. H. Vineyard, *Journal of Physics and Chemistry of Solids* **3**, 121 (1957).
- [11] J. Lu and Y. Li, *Journal of Materials Science: Materials in Electronics* **32**, 9736 (2021).
- [12] M. Imada, A. Fujimori, and Y. Tokura, *Reviews of Modern Physics* **70**, 1039 (1998).
- [13] E. Dagotto, *Science* **309**, 257 (2005).
- [14] J. Ngai, F. Walker, and C. Ahn, *Annual Review of Materials Research* **44**, 1 (2014).
- [15] H. Han, A. Sharma, H. L. Meyerheim, J. Yoon, H. Deniz, K.-R. Jeon, A. K. Sharma, K. Mohseni, C. Guillemand, M. Valvidares, P. Gargiani, and S. S. P. Parkin, *ACS Nano* **16**, 6206 (2022).
- [16] A. Muñoz, C. de la Calle, J. A. Alonso, P. M. Botta, V. Pardo, D. Baldomir, and J. Rivas, *Physical Review B* **78**, 054404 (2008).
- [17] C. Mitra, T. Meyer, H. N. Lee, and F. A. Reboredo, *The Journal of Chemical Physics* **141**, 084710 (2014).
- [18] X. He, Y. Zhu, and Y. Mo, *Nature Communications* **8**, 15893 (2017).
- [19] P. E. Blöchl, *Physical Review B* **50**, 17953 (1994).
- [20] G. Kresse and D. Joubert, *Physical Review B* **59**, 1758 (1999).
- [21] G. Kresse and J. Furthmüller, *Computation Materials Science* **6**, 15 (1996).
- [22] G. Kresse and J. Furthmüller, *Physical Review B* **54**, 11169 (1996).
- [23] J. P. Perdew, K. Burke, and M. Ernzerhof, *Physical Review Letters* **77**, 3865 (1996).
- [24] A. I. Liechtenstein, V. I. Anisimov, and J. Zaanen, *Physical Review B* **52**, R5467 (1995).
- [25] N. Lu, Z. Zhang, Y. Wang, H.-B. Li, S. Qiao, B. Zhao, Q. He, S. Lu, C. Li, Y. Wu, M. Zhu, X. Lyu, X. Chen, Z. Li, M. Wang, J. Zhang, S. C. Tsang, J. Guo, S. Yang, J. Zhang, K. Deng, D. Zhang, J. Ma, J. Ren, Y. Wu, J. Zhu, S. Zhou, Y. Tokura, C.-W. Nan, J. Wu, and P. Yu, *Nature Energy* **7**, 1208 (2022).
- [26] G. Henkelman, B. P. Uberuaga, and H. Jónsson, *The Journal of Chemical Physics* **113**, 9901 (2000).
- [27] G. Henkelman and H. Jónsson, *The Journal of Chemical Physics* **113**, 9978 (2000).
- [28] K. Parlinski, Z. Q. Li, and Y. Kawazoe, *Physical Review Letters* **78**, 4063 (1997).
- [29] A. Togo and I. Tanaka, *Scripta Materialia* **108**, 1 (2015).
- [30] M. A. Korotin, S. Y. Ezhov, I. V. Solovyev, V. I. Anisimov, D. I. Khomskii, and G. A. Sawatzky, *Physical Review B* **54**, 5309 (1996).
- [31] E. Zintl, A. Harder, and B. Dauth, *Zeitschrift für Elektrochemie und angewandte physikalische Chemie* **40**, 588 (1934).
- [32] Y. N. Zhuravlev and O. S. Obolonskaya, *Journal of Structural Chemistry* **51**, 1005 (2010).
- [33] R. Lin, E. Hu, M. Liu, Y. Wang, H. Cheng, J. Wu, J.-C. Zheng, Q. Wu, S. Bak, X. Tong, R. Zhang, W. Yang, K. A. Persson, X. Yu, X.-Q. Yang, and H. L. Xin, *Nature Communications* **10**, 10.1038/s41467-019-09248-0 (2019).
- [34] A. O. Boev, M. Y. Arsentev, S. S. Fedotov, A. M. Abakumov, and D. A. Aksyonov, *Physical Review Materials* **8**, 055403 (2024).
- [35] J. Koettgen, T. Zacherle, S. Grieshammer, and M. Martin, *Physical Chemistry Chemical Physics* **19**, 9957 (2017).
- [36] C. Wang, K. Fu, S. P. Kammampata, D. W. McOwen, A. J. Samson, L. Zhang, G. T. Hitz, A. M. Nolan, E. D. Wachsmann, Y. Mo, V. Thangadurai, and L. Hu, *Chemical Reviews* **120**, 4257 (2020).
- [37] A. Manthiram, X. Yu, and S. Wang, *Nature Reviews Materials* **2**, 16103 (2017).
- [38] Z. Wu, X. Li, C. Zheng, Z. Fan, W. Zhang, H. Huang, Y. Gan, Y. Xia, X. He, X. Tao, and J. Zhang, *Electrochemical Energy Reviews* **6**, 10 (2023).